J|A|C|S
ARTICLES

Published on Web 05/18/2009

Indirect Effects Modulating the Interaction between DNA and a Cytotoxic Bisnaphthalimide Reveal a Two-Step Binding Process

Luis González-Bulnes and José Gallego*

Centro de Investigación Príncipe Felipe, Avda. Autopista del Saler 16, 46012 Valencia, Spain

Received February 26, 2009; E-mail: jgallego@cipf.es

Abstract: The sequence-specific structural and dynamic properties of double-helical DNA play important roles in many biological processes involving DNA recognition. Using a combination of NMR spectroscopy, surface plasmon resonance, and UV thermal denaturation experiments, we have investigated how sequences not making direct contact with the drug modulate the interaction between the cytotoxic agent elinafide and its preferred bisintercalation sites on double-helical DNA. Our combined data are consistent with two superposed interactions, one process involving ligand binding to the DNA duplex with nanomolar dissociation constants and another process of ring intercalation characterized by faster dissociation rates and substantially higher dissociation constants in some cases. The sequence of the base pairs flanking the bisnaphthalimide binding tetranucleotides influence both events through indirect readout effects, but these effects appear to be particularly relevant for the second (intercalation) process. The most unfavorable sequences contain specifically oriented A-tracts that oppose DNA intercalation of the naphthalimide rings, as reflected by strikingly different thermal stability and thermodynamic binding profiles. The complexes of elinafide with these sequences are characterized by poor DNA−naphthalimide and DNA−DNA stacking interactions and by enhanced dynamics of the ligand's intercalated rings and of the base pairs forming the tetranucleotide binding site.

Introduction

The binding of proteins and small molecules to their target sites in double-helical DNA is often dictated by the sequence-dependent structural and dynamic properties of this polymer. In studies of DNA−protein interactions, this recognition mechanism is termed indirect readout, as opposed to the direct interactions of the protein side chains with specific DNA functional groups.[1] The indirect recognition of DNA has both structural and dynamic origins. If the bound DNA conformation is close to the intrinsic shape of the free DNA, the energetic cost of DNA deformation will be smaller and that sequence will be favored for binding. In addition, the conformational dynamics of a target sequence may facilitate (or preclude) the trapping by the ligand of a short-lived conformation necessary to initiate the binding process. These effects have been shown to determine the sequence-specific binding to DNA of many proteins including bacteriophage 434 repressor,[2] TATA box binding protein,[3] and human papillomavirus E2,[4] among others.

Indirect sequence effects are also important for drug−DNA recognition, particularly when binding involves selecting a DNA conformation that is far from the ground state(s) of the polymer, such as those induced by threading agents (requiring large conformational changes for binding and dissociation[5−7]), intercalators,[8] and, to a lesser extent, groove-binding agents.[9] Indirect effects are potentially relevant for drug design, because they could be exploited to increase the binding specificity of cytotoxic or antibacterial agents, a question of paramount importance in this area. DNA deformation energies have recently been estimated for a set of DNA-binding drugs,[10] but reports studying the mechanisms of indirect sequence effects on drug−DNA interactions are much scarcer relative to those focused on protein−DNA complexes.

In fact, many aspects of DNA structure and dynamics that are relevant for the indirect recognition of DNA sequence by both proteins and small molecules remain unclear. NMR and X-ray structures are time- and population-averaged, and although NMR spectroscopy is well suited to provide dynamic information over a broad range of time scales, the methods available to study nucleic acid dynamics are less well developed than those for proteins, and some relevant time scales (particularly the microsecond to millisecond range) remain difficult to study. The shortcomings are particularly acute when trying to char-

(1) Drew, H. R.; Travers, A. A. *Cell* **1984**, *37*, 491–502.
(2) Koudelka, G. B.; Mauro, S. A.; Ciubotaru, M. *Prog. Nucleic Acids Res. Mol. Biol.* **2006**, *81*, 143–77.
(3) Faiger, H.; Ivanchenko, M.; Cohen, I.; Haran, T. E. *Nucleic Acids Res.* **2006**, *34*, 104–19.
(4) Zhang, Y.; Xi, Z.; Hegde, R. S.; Shakked, Z.; Crothers, D. M. *Proc. Natl. Acad. Sci. U.S.A.* **2004**, *101*, 8337–41.
(5) Fox, K. R.; Brassett, C.; Waring, M. J. *Biochim. Biophys. Acta* **1985**, *840*, 383–92.
(6) Tanious, F. A.; Yen, S. F.; Wilson, W. D. *Biochemistry* **1991**, *30*, 1813–9.
(7) Onfelt, B.; Lincoln, P.; Norden, B. *J. Am. Chem. Soc.* **2001**, *123*, 3630–7.
(8) Qu, X.; Ren, J.; Riccelli, P. V.; Benight, A. S.; Chaires, J. B. *Biochemistry* **2003**, *42*, 11960–7.
(9) Degtyareva, N. N.; Fresia, M. J.; Petty, J. T. *Biochemistry* **2007**, *46*, 15136–43.
(10) Arauzo-Bravo, M. J.; Sarai, A. *Nucleic Acids Res.* **2008**, *36*, 376–86.

acterize transient, short-lived intermediates that may be needed for binding or dissociation. Molecular dynamics simulations are beginning to provide some answers in this respect, but the current simulation limit is approximately 1 μs,[11,12] and DNA force field descriptions are still being refined.[11]

The naphthalimides[13] are a family of DNA intercalators that raise sustained interest due to their antitumor properties.[14−16] Elinafide (abbreviated as LU)[17] is a member of this family that contains two unsubstituted naphthalimide rings joined together by a flexible aminoalkyl chain (Figure 1A). The two protonated amino groups of the linker recognize the electronegative N7 and O6 groups of guanine in the major groove, and the naphthalimide rings preferentially intercalate into mixed TpG (CpA) steps.[18,19] In the resulting TGCA binding tetranucleotide, the two A·T pairs flank the outer side of the drug rings, and the GpC dinucleotide interacting with the aminoalkyl linker is sandwiched by the inner side of the rings[19] (Figure 1B).

Despite the small size of its aromatic rings, elinafide, like other intercalating agents, induces groove widening and unwinding of the base pairs,[19] making its interaction with DNA susceptible to being modulated by indirect effects. In addition, the TGCA-intercalated rings of elinafide have previously been found to exchange between two intercalated conformations via 180° rotating motions that do not affect the aminoalkyl linker atoms bound to the major groove.[10] Since these ring flipping motions depend on the sequence of the base pairs flanking the TGCA binding site,[20] they can provide additional information on the mechanism of indirect effects on the DNA−elinafide interaction.

In the present study, we have used a combination of NMR spectroscopy, surface plasmon resonance (SPR), and UV thermal denaturation experiments to study the binding parameters, structure, and dynamics of a series of DNA−elinafide complexes flanked by different sequences. Our data reveal that the sequence of the base pairs flanking the bisnaphthalimide binding sites can cause 10-fold variations of the DNA−elinafide dissociation constants through indirect readout effects. The most unfavorable flanking sequences oppose intercalation of the naphthalimide rings, and the complexes of the drug with these sequences exhibit weaker intra- and intermolecular stacking interactions and increased DNA and ligand dynamics.

Materials and Methods

Sample Preparation. After purification of the DNA oligonucleotides using a methodology based on gel electrophoresis, ethanol precipitation, and dialysis, six self-complementary DNA duplexes (Figure 1C) were titrated with elinafide by 1D NMR spectroscopy using the slowly exchanging free and bound DNA aromatic resonances (Figure S1, Supporting Information). The final NMR samples contained 0.2−0.8 mM complex and were microdialyzed in 20 mM sodium phosphate, pH 6.9, 0.2 mM ethylenediaminetetraacetic acid (EDTA), and 150 or 1000 mM NaCl aqueous solutions. The samples for UV thermal denaturation experiments contained 0.5 ODU mL^{-1} (approximately 2 μM) of free duplex or NMR complex and were dissolved in similar solutions. For the SPR experiments, three 5′-biotin-labeled hairpins (Figure 1C) were purchased HPLC-purified from Microsynth AG and microdialyzed in HBS-EP buffer (10 mM *N*-2-hydroxyethylpiperazine-*N*′-2-ethanesulfonic acid (HEPES), pH 7.4, 150 mM NaCl, 3 mM EDTA, and 0.005% (v/v) surfactant P20) prior to immobilization.

NMR Spectroscopy. NMR spectra were acquired on a temperature-calibrated Bruker 600 MHz spectrometer equipped with a TCI HCN cryoprobe, processed with Topspin 1.3 (Bruker Biospin) and analyzed using Topspin 1.3 or Sparky 3.110.[21] Each DNA−bisnaphthalimide complex was analyzed using ^1H_2O WATERGATE NOESY at 8 °C and series of ^2H_2O NOESYs (at 8 and 25 °C) collected without interruption at several mixing times (typically 0, 4, 8, 12, 20, 80, and 250 ms), together with ROESY, and dqf-COSY or TOCSY experiments, all with recycle delays of 2 s. Imino proton longitudinal relaxation times, T_1, were determined at 8 °C from inversion recovery experiments comprising a selective 2000−2500 ms 180° Gaussian pulse for inversion, followed by a variable delay and a 4500−5000 ms 90° Gaussian observe pulse. The carrier frequency was centered on the imino proton region, and the spectral width was set to 3000 Hz. All elinafide resonances and all of the aromatic, H1′, H3′, H2′, and H2″ DNA resonances were assigned in each of the complexes studied. All sequences formed the self-complementary duplexes shown in Figure 1C.

Bisnaphthalimide Ring Rotation Rates, k_{rot}, and Activation Parameters. Values of k_{rot} were determined by NMR spectroscopy at an average of six different temperatures per complex, ranging from 8 to 48 °C, using a combination of NOESY data at low mixing times and line shape analyses.[20] Values of $\Delta H^{\ddagger}_{rot}$, $\Delta S^{\ddagger}_{rot}$ and $\Delta G^{\ddagger}_{rot}$ were obtained from the Eyring dependence of the rate constants with temperature.[20]

Intercalation Dissociation Rates, k_d^{int}. These rates were determined from NOESY experiments at low mixing times using well-resolved aromatic or H1′ DNA resonances of intercalated complexes and their cross-peaks to residual unstacked DNA.[20]

Base-Pair Lifetimes, τ_{op}, and Opening Rates, k_{op}. These were obtained by measuring the exchange times of G and T imino protons with solvent as a function of base concentration, [B],[22] and extrapolating to infinite [B]:

$$\tau_{ex} = \tau_{op} + \frac{1}{\alpha K_d k_i [B]}$$

A plot of τ_{ex} versus 1/[B] yields a straight line where the *y*-intercept is $\tau_{op} = 1/k_{op}$ and the slope is $1/(\alpha K_d k_i)$, where K_d is the dissociation constant for the base pair, k_i is the proton transfer rate from the mononucleoside, and α is an accessibility parameter. For these experiments the DNA−elinafide complexes were microdialyzed in aqueous buffers containing 3 mM sodium borate, pH 8.8, 150 mM NaCl, and 0.1 mM EDTA and were titrated with a 1.8 M pH 8.8 stock solution of ammonia as the base catalyst, keeping the sample pH at approximately 8.8 after each base addition. The imino proton exchange times at different ammonia concentrations, τ_{ex}, were obtained from the longitudinal relaxation times, T_1, determined by inversion recovery experiments (described above), after subtracting the effect of longitudinal relaxation in the absence of added catalyst, T_1°:

(11) Perez, A.; Luque, F. J.; Orozco, M. *J. Am. Chem. Soc.* **2007**, *129*, 14739–45.
(12) Mura, C.; McCammon, J. A. *Nucleic Acids Res.* **2008**, *36*, 4941–55.
(13) Braña, M. F.; Castellano, J. M.; Roldan, C. M.; Santos, A.; Vazquez, D.; Jimenez, A. *Cancer Chemother. Pharmacol.* **1980**, *4*, 61–6.
(14) Bailly, C.; Carrasco, C.; Joubert, A.; Bal, C.; Wattez, N.; Hildebrand, M. P.; Lansiaux, A.; Colson, P.; Houssier, C.; Cacho, M.; Ramos, A.; Braña, M. F. *Biochemistry* **2003**, *42*, 4136–50.
(15) Carrasco, C.; Joubert, A.; Tardy, C.; Maestre, N.; Cacho, M.; Braña, M. F.; Bailly, C. *Biochemistry* **2003**, *42*, 11751–61.
(16) Van Quaquebeke, E.; Mahieu, T.; Dumont, P.; Dewelle, J.; Ribaucour, F.; Simon, G.; Sauvage, S.; Gaussin, J. F.; Tuti, J.; El Yazidi, M.; Van Vynckt, F.; Mijatovic, T.; Lefranc, F.; Darro, F.; Kiss, R. *J. Med. Chem.* **2007**, *50*, 4122–34.
(17) Braña, M. F.; Castellano, J. M.; Moran, M.; Perez de Vega, M. J.; Perron, D.; Conlon, D.; Bousquet, P. F.; Romerdahl, C. A.; Robinson, S. P. *Anti-Cancer Drug Des.* **1996**, *11*, 297–309.
(18) Bailly, C.; Brana, M.; Waring, M. J. *Eur. J. Biochem.* **1996**, *240*, 195–208.
(19) Gallego, J.; Reid, B. R. *Biochemistry* **1999**, *38*, 15104–15.
(20) Gallego, J. *Nucleic Acids Res.* **2004**, *32*, 3607–14.
(21) Goddard, T. D.; Kneller, D. G. University of California, San Francisco, CA.
(22) Guéron, M.; Leroy, J.-L. *Methods Enzymol.* **1995**, *261*, 383–413.

$$\frac{1}{\tau_{ex}} = \frac{1}{T_1} - \frac{1}{T_1^\circ}$$

UV Thermal Denaturation Experiments. The thermal denaturation of the unbound DNA duplexes and DNA−bisnaphthalimide complexes was monitored by measuring the UV absorbance at 260 nm as a function of temperature in a Varian Cary 300 spectrophotometer. The temperature was raised from 10 to 90 °C at a gradient of 0.5 °C min^{-1} and subsequently decreased at the same rate to evaluate the reversibility of the process.

Surface Plasmon Resonance (SPR). These experiments were carried out using a Biacore T100 optical biosensor system and a four-channel streptavidin-derivatized Series S SA chip. *DNA immobilization*. A 25 nM HBS-EP solution of each of the three 5′ biotin-labeled hairpins was manually injected at 1 μL/min into one flow cell of the chip, leaving the remaining cell blank for

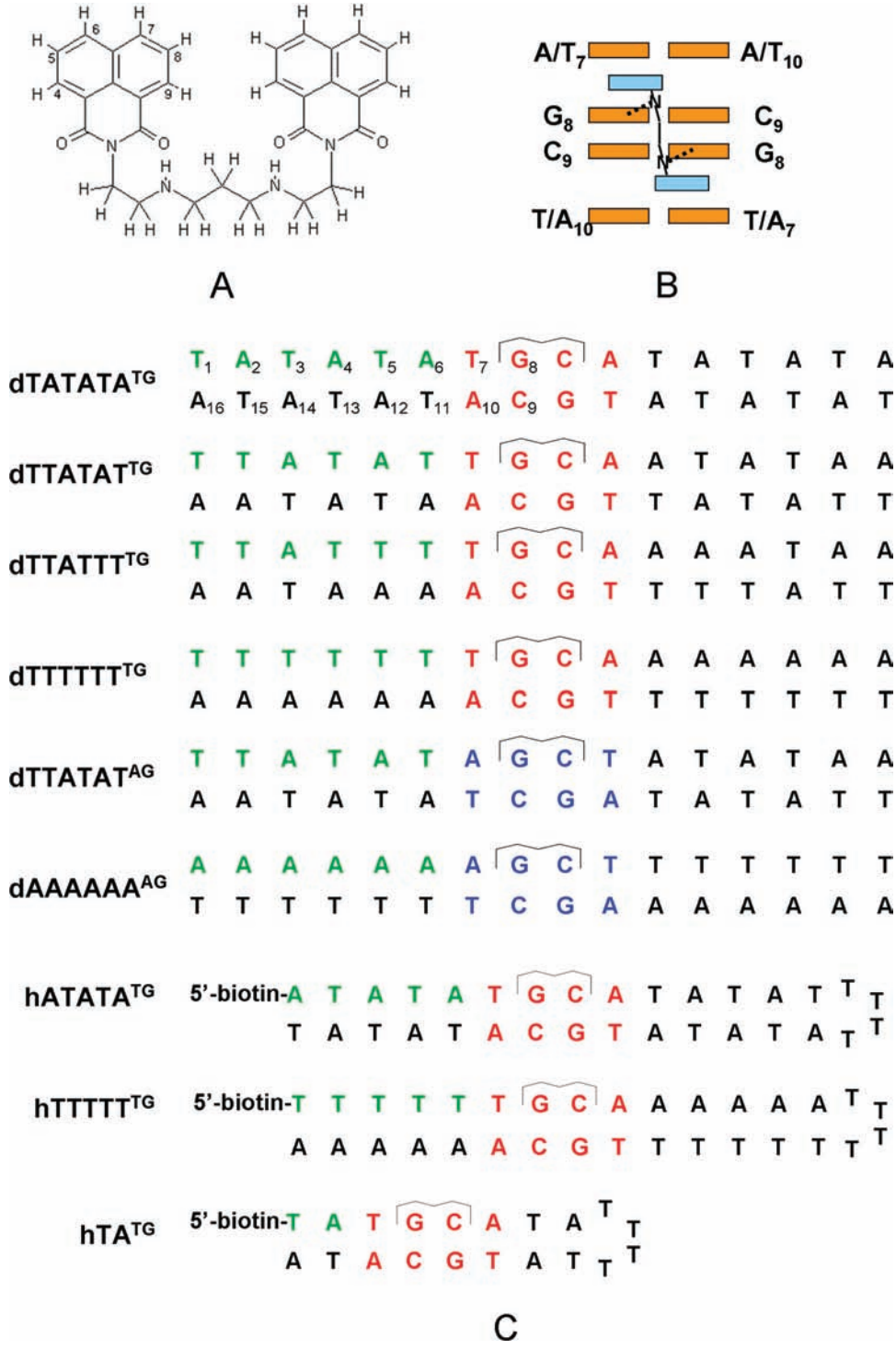

Figure 1. Elinafide and DNA−elinafide complexes. (A) Chemical structure of elinafide. (B) Schematic representation of a DNA−elinafide complex. The interactions between the amino groups of the elinafide linker and the O6 and N7 atoms of guanine in the major groove are represented with dashed lines. (C) DNA−elinafide complexes analyzed in this study: six self-complementary 16 base-pair duplexes and three 5′-biotinylated hairpins. The invariant bisnaphthalimide TGCA and AGCT binding sites are indicated with red and blue colors, respectively, whereas the 5′ flanking sequences are highlighted in green.

Table 1. Effect of Flanking Sequence on the Affinity, Kinetics and Dynamics of the Interaction between Elinafide and Self-Complementary DNA Duplexes: Free (T_m^f) and Bound (T_m^b) DNA Melting Temperatures, Elinafide-Induced DNA Thermal Stabilizations (ΔT_m), DNA−Naphthalimide Intercalation Dissociation Rates (k_d^{int}) and Naphthalimide Ring Rotation Rates (k_{rot}) at 25 °C

complex[a]	T_m^f (°C)	T_m^b (°C)	ΔT_m (°C)	k_d^{int} (s^{-1})	k_{rot}[c] (s^{-1})
		TGCA Complexes			
$dTATATA^{TG}$	46	52	6	3.8 ± 0.6	15
$dTTATAT^{TG}$	45	50	5	0.9 ± 0.1	13
$dTTATTT^{TG}$	48	50	2	*b*	32
$dTTTTTT^{TG}$	55	55	0	2.7 ± 0.9	30
		AGCT Complexes			
$dTTATAT^{AG}$	42	50	8	*b*	13
$dAAAAAA^{AG}$	49	54	5	*b*	21

[a] The sequences of the complexes are shown in Figure 1C, and the DNA:elinafide equivalent ratios are (as required by NMR titrations): $dTATATA^{TG}$, 1:1.1; $dTTATAT^{TG}$, 1:1.4; $dTTATTT^{TG}$, 1:1.6; $dTTTTTT^{TG}$, 1:2.5; $dTTATAT^{AG}$, 1:1.5; $dAAAAAA^{AG}$, 1:1.5. The thermal denaturation experiments were repeated at least two times for each system, and the average standard error for T_m and ΔT_m values is 1 °C. [b] Not measured due to lack of appropriate peaks. [c] Calculated from the Eyring plots at $T = 25$ °C (Figure 5A and Figure S4, Supporting Information). The average error for experimental k_{rot} measurements is 10% (Figure 5A and Figure S4, Supporting Information). The $\Delta G^{\ddagger}_{rot}$ values obtained from the Eyring plots range from 15.4 ($dTTATTT^{TG}$) to 16.0 ($dTTATAT^{AG}$) kcal mol^{-1}.

referencing. We immobilized approximately 300 response units (RU) of 32-nucleotide hairpins and 400 RUs of 20-nucleotide hairpin (Figure 1C). The flow cells were previously conditioned by applying several consecutive injections of a 1 M NaCl, 50 mM NaOH solution until a stable baseline was observed, followed by extensive washing with HBS-EP buffer. *SPR Experiments*. We carried out steady-state binding analyses at five different temperatures (10, 18, 25, 32, and 40 °C) by injecting different elinafide concentrations over the immobilized DNA surfaces for a 15 min period at a flow rate of 20 μL/min. The elinafide concentrations ranged from 0.5 nM to 0.15 μM in MES-15 solutions (10 mM 2-(*N*-morpholino)ethanesulfonic acid (MES), pH 6.25, 150 mM NaCl, 1 mM EDTA, and 0.005% P20). The DNA surface was regenerated by buffer flow over a 30 min period.

Determination of DNA−Elinafide Dissociation Constants. The instrument response (RU) in the steady-state region is proportional to the amount of bound elinafide and was determined for each drug concentration injected. The dissociation constants, K_d, were determined by fitting the sensorgrams to one-site or two-site equations, using the Biacore T100 evaluation software:

$$RU = \frac{RU_{max} C}{1 + K_d C} + RI \quad \text{(one-site)}$$

$$RU = \frac{RU_{max1} C}{1 + K_{d1} C} + \frac{RU_{max2} C}{1 + K_{d2} C} + RI \quad \text{(two-site)}$$

where C is the concentration of free elinafide in equilibrium with the complex (which equals the elinafide concentration in the flow solution), RU_{max} is the maximum response in the steady-state region, and RI is an offset term accounting for the bulk refractive index contribution of the sample. In these models, K_d, RU_{max}, and RI are adjustable parameters, and the stoichiometry of each binding site was determined by comparing the fitted RU_{max} values with the predicted ones, calculated from the molecular weights of DNA and elinafide and the amount of DNA in the flow cell.[23] Association and dissociation rate constants were obtained from global kinetic fits, using low concentration sensorgrams and a one-site model including a mass transfer term.

Results

We studied by NMR spectroscopy and UV thermal denaturation experiments complexes of elinafide with six 16-base-pair self-complementary duplexes containing TGCA and AGCT binding sites (these complexes will be hereafter identified with the sequence flanking the 5′ side of the binding tetranucleotide followed by TG or AG superscripts designating TGCA and AGCT binding sites, respectively). The series included four complexes containing a TGCA binding site flanked by alternating AT pairs ($dTATATA^{TG}$), mixed AT pairs ($dTTATAT^{TG}$), short A-tracts on 3′ ($dTTATTT^{TG}$), and continuous A-tracts on 3′ ($dTTTTTT^{TG}$) and two complexes containing an AGCT binding site flanked by mixed AT pairs ($dTTATAT^{AG}$) and continuous A-tracts on 5′ ($dAAAAAA^{AG}$) (Figure 1C).

Analysis of the NMR data confirmed that the two rings of elinafide bisintercalate into TGCA and AGCT from the major groove in all complexes, as observed previously for TGCA sites.[19,20] Since the chemical environment of the naphthalimide rings and linker is the same within the TGCA and AGCT series (see Figure 1C), the observed differences must be due to indirect effects linked to the structural preferences or conformational fluctuations of the DNA molecules.

Intercalation Constants. DNA−elinafide titrations were carried out by NMR spectroscopy using the slowly exchanging free and bound DNA aromatic resonances indicating intercalation of the naphthalimide rings. These initial experiments revealed a significant difference for the TGCA complex flanked by continuous A-tracts on 3′ ($dTTTTTT^{TG}$). This sequence required approximately 2 equiv of ligand for full intercalation of the naphthalimide rings at NMR concentrations, whereas the other sequences required approximately one (Table 1 and Figure S1, Supporting Information). Analysis of the NMR and SPR data (see below) indicates that there are no interactions of elinafide with the flanking A-tracts of $dTTTTTT^{TG}$. Based on these results (Figure S1, Supporting Information), we estimate an *intercalation* dissociation constant of approximately 3×10^{-4} M for $dTTTTTT^{TG}$, significantly higher than the intercalation constants of the other complexes.

UV Thermal Stabilizations. The UV melting temperatures of complexes between DNA and intercalative agents are usually higher relative to the isolated duplexes, and this stabilization has been proposed to be proportional to the affinity of the DNA−ligand interaction.[24,25] The sequences flanking the TGCA and AGCT sites have a large impact on the duplex thermal stabilizations induced by elinafide (Table 1 and Figure 2A). If we compare the TGCA series first, ΔT_m is highest (6 °C) for the alternating $dTATATA^{TG}$ complex, decreases progressively

(23) Nguyen, B.; Tanious, F. A.; Wilson, W. D. *Methods* **2007**, *42*, 150–61.
(24) Crothers, D. M. *Biopolymers* **1971**, *10*, 2147–60.
(25) Wilson, W. D.; Tanious, F. A.; Fernandez-Saiz, M.; Rigl, C. T. *Methods Mol. Biol.* **1997**, *90*, 219–40.

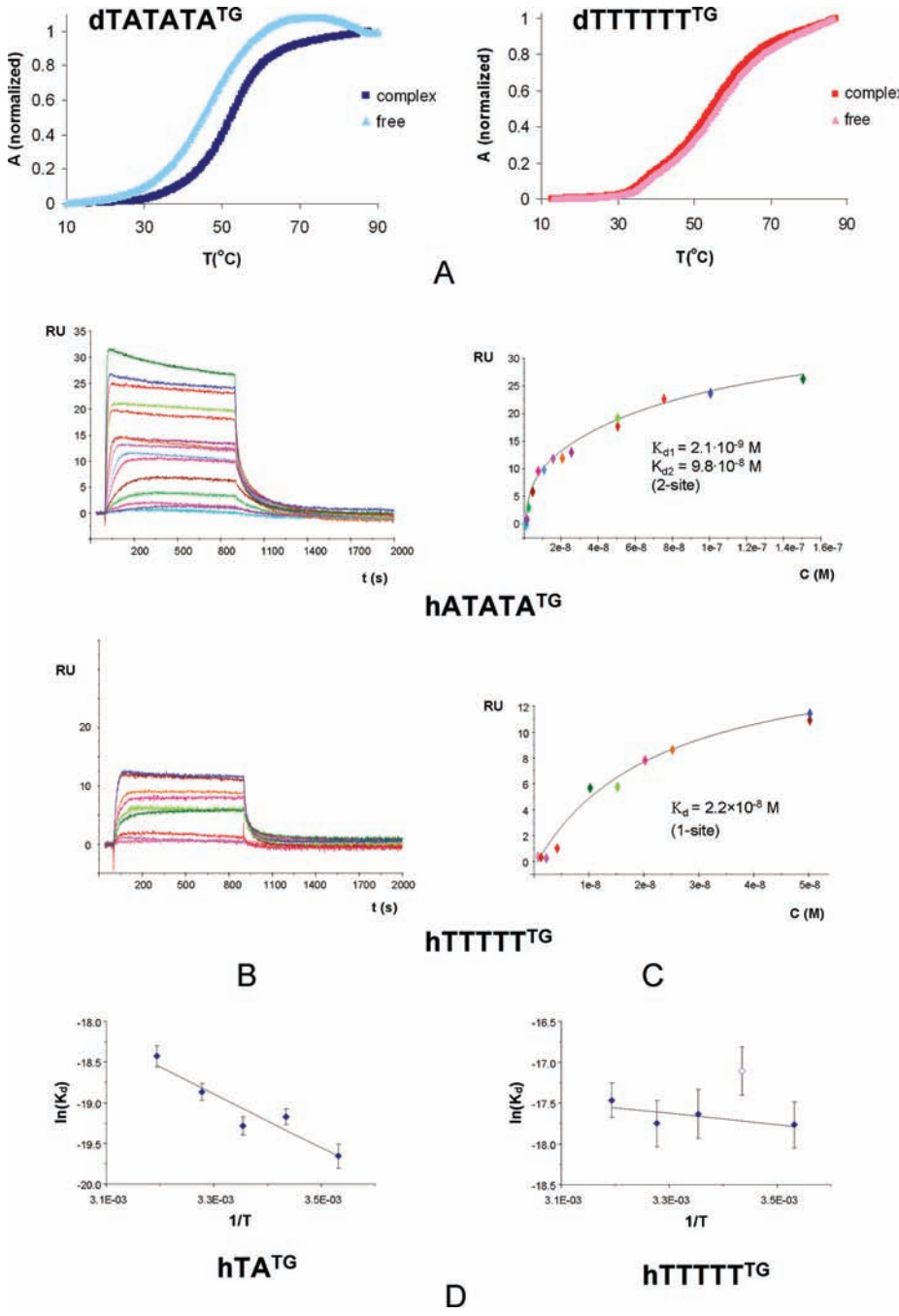

Figure 2. UV thermal denaturation and SPR experiments. (A) UV melting curves of dTATATA^{TG} and dTTTTTT^{TG} in the absence and presence of 1.1 and 2.5 equiv of elinafide, respectively. All samples contained 2 μM DNA. (B) SPR sensorgrams for the interaction of elinafide with hATATA^{TG} and hTTTTT^{TG} at 25 °C. For both systems, the elinafide concentrations range from 0.5×10^{-9} (lowest curve) to 1.5×10^{-7} M (highest curve). Similar quantities of hairpin (approximately 300 RUs) were immobilized on the SPR chip. (C) Steady-state binding analyses for hATATA^{TG} and hTTTTT^{TG}. The RU values from the steady-state regions of the sensorgrams are plotted against the concentration of free elinafide (*C*, M). The data were adjusted with a two-site binding function for hATATA^{TG} and a one-site function for hTTTTT^{TG} (see Materials and Methods). (D) van't Hoff plots comparing the hTA^{TG} and hTTTTT^{TG} SPR dissociation constants (K_d's, M) as a function of temperature (*T*, K). Both sets of constants were determined using a one-site model.

in dTTATAT^{TG} and dTTATTT^{TG}, and becomes negligible for the dTTTTTT^{TG} complex flanked by continuous A-tracts on 3′ (see Table 1 and Figure 2A). The observed difference in ΔT_m would translate into an approximately 10 000-fold difference between the dTATATA^{TG}− and dTTTTTT^{TG}−elinafide binding affinities calculated using this parameter (Table S1, Supporting Information).

A-tracts flanking AGCT complexes on 5′ also have unfavorable effects, although to a lesser extent: ΔT_m halves for the dAAAAAA^{AG} complex relative to dTTATAT^{AG} (Table 1). Comparison of dTTTTTT^{TG} and dAAAAAA^{AG} indicates that the indirect effect of the A-tract depends on its orientation with respect to the complex: A-tracts located on the 3′ side of the complexes (as in dTTTTTT^{TG}) have a more pronounced effect on ΔT_m than A-tracts located on the other side.

DNA−Elinafide Dissociation Constants. In order to obtain additional binding data, we carried out SPR experiments with two 32-nucleotide hairpins containing a TGCA site flanked by alternating AT pairs or continuous A-tracts on 3′ (these will be identified as explained above as hATATA^{TG} and hTTTTT^{TG},

Table 2. SPR Analysis of the Interaction between Elinafide and the DNA Hairpins hTA^{TG}, hATATA^{TG}, and hTTTTT^{TG}

(A) Equilibrium Dissociation Constants (K_d), Association (k_a) and Dissociation (k_d) Rates, and Binding Stoichiometries at 25 °C

TGCA complex[a]	K_d (M)[b]	k_a (M^{-1} s^{-1})	k_d (s^{-1})	k_d/k_a (M)	n[c]	m[c]
hTA^{TG}	4.2×10^{-9}	5.5×10^{6}	2.2×10^{-2}	4.2×10^{-9}	1	1
hATATA^{TG}[d]	2.1×10^{-9} (9.8×10^{-8})	2.7×10^{6}	1.1×10^{-2}	3.9×10^{-9}	2	3
hTTTTT^{TG}	2.2×10^{-8}	7.6×10^{5}	1.8×10^{-2}	2.3×10^{-8}	1	1

(B) Thermodynamic Parameters at 25 °C[e]

TGCA complex[a]	ΔH (kcal/mol)	$T\Delta S$ (kcal/mol)
hTA^{TG}	-6.7 ± 1.3	4.7 ± 1.2
hATATA^{TG}[d]	-6.0 ± 2.4	5.6 ± 2.4
hTTTTT^{TG}	-1.4 ± 1.0	9.3 ± 0.9

[a] The hairpin sequences are shown in Figure 1C. [b] The standard errors of the K_d's are shown in Figure 2 and Figure S2, Supporting Information. [c] Parameters n and m indicate the number of binding sites per hairpin and the total number of elinafide molecules binding to each hairpin, respectively. [d] For hATATA^{TG}, the equilibrium K_{d1} and K_{d2} dissociation constants were determined using a two-site model, and the second-site K_{d2} is indicated in parentheses; k_a, k_d, and k_d/k_a were calculated at low elinafide concentrations using a one-site kinetic model; ΔH and $T\Delta S$ were calculated from the temperature-dependence of the first-site equilibrium K_{d1}'s. [e] Calculated from the temperature dependence of the SPR equilibrium K_d values.

where h designates a hairpin). A third 20-nucleotide alternating AT hairpin (hTA^{TG}) lacking possible secondary binding sites in the flanking regions was also analyzed as a control (Figure 1C). Indeed, comparison of the experimental and predicted maximum responses (RU_{max}) indicated binding of one drug molecule to hTA^{TG} and hTTTTT^{TG} and of three drug molecules to hATATA^{TG}, and the best steady-state fits were obtained using a one-site binding model for hTA^{TG} and hTTTTT^{TG}, and an independent two-site model for hATATA^{TG} (Figure 2B and Figure S2, Supporting Information). These data indicate that elinafide binds to two equivalent low-affinity sites in the flanking AT sequences of hATATA^{TG} after the high-affinity TGCA site is saturated. This effect is not seen in hTTTTT ^{TG} nor in hTA^{TG} due to the shortened stem.

A comparison of the elinafide binding affinities for the TGCA sites of hTA^{TG}, hATATA^{TG}, and hTTTTT^{TG} reveals that whereas the equilibrium dissociation constants (K_d) of the alternating hTA^{TG} and hATATA^{TG} hairpins are as expected very similar (4.2×10^{-9} and 2.1×10^{-9} M, respectively), the K_d for the A-tract-flanked TGCA hTTTTT^{TG} hairpin is approximately 10-fold higher (Table 2A). Note that these DNA−elinafide K_d values are substantially lower than the dissociation constants calculated from the ΔT_m values of equivalent duplexes (Table S1, Supporting Information) and the NMR intercalation dissociation constant estimated for dTTTTTT^{TG}. In particular, the discrepancy between the SPR-determined DNA−elinafide K_d values and the NMR (intercalation) and ΔT_m dissociation constants is approximately 10 000-fold for the dTTTTTT^{TG} and hTTTTT^{TG} TGCA complexes flanked by continuous A-tracts on 3′ (Table 2A and Figure S1 and Table S1, Supporting Information).

Thermodynamic Binding Profiles. The enthalpy and entropy components of the interaction between elinafide and hTA^{TG}, hATATA^{TG}, and hTTTTT^{TG} were obtained from the temperature-dependence of the SPR equilibrium K_d values (Figure 2C, Figure S2, Supporting Information, and Table 2B). The results indicate that the lower affinity of elinafide for hTTTTT^{TG} is mainly due to a reduced binding enthalpy. This term is five-times less negative in hTTTTT^{TG}, containing a TGCA site flanked by A-tracts, relative to the hTA^{TG} and hATATA^{TG} hairpins containing TGCA sites flanked by alternating AT sequences.

Structural Effects. As previously determined,[19] the TGCA−elinafide complexes exhibit diagnostic NOEs between LU H9 and C9 H5, LU H7 and A10 H1′, LU H5 and A10 H2, LU H4 and G8 H8, and LU H4 and T7 H1′ among others, indicating bisintercalation of the naphthalimide rings into the T7·A10−G8·C9 steps from the major groove (Figures 3 and 4). Comparison of the NOESY spectra of dTATATA^{TG} and dTTTTTT^{TG} reveals that whereas the NOEs involving G8 and C9 are approximately similar in both complexes (e.g., cross-peak k in Figure 3A,B), the NOEs with the H1′ and H2 protons of the outer T7·A10 pair are substantially weaker or nondetectable in dTTTTTT^{TG} (Figure 3B, cross-peak l). This is in contrast to dTATATA^{TG}, which is characterized by medium-intensity LU H6, H7−A10 H1′ NOEs (Figure 3A, cross-peaks l and m) indicating stacking of the naphthalimide on A10[19] (Figure 4). The intramolecular NOEs between the adenine H2 protons and the H1′ protons of sequential and cross-strand nucleotides are stronger in dTTTTTT^{TG} relative to dTATATA^{TG} (compare the green-labeled cross-peaks in Figure 3A,B), indicating that the T1·A16−T6·A11 segment flanking the TGCA site in dTTTTTT^{TG} retains the conformation typical of A-tracts characterized by negative base inclination and a compressed minor groove.[26−31] However, A10 H2 and H8 of dTTTTTT^{TG} are broadened (Figure 3B), and A10 H2 gives rise to weaker NOEs with the H2 and H1′ protons of A11, pointing to a disruption of the A-tract structure of this complex at the T7·A10−T6·A11 step.

The AGCT−elinafide complexes exhibit equivalent interactions with the aromatic and sugar protons of the tetranucleotide binding site, indicating similar bisintercalation of the drug rings into the A7·T10−G8·C9 steps from the major groove (Figure S3, Supporting Information). The strong LU H4−A7 H1′ and LU H5, H6−A7 H2 NOEs observed in the dTTATAT^{AG} complex reflect stacking of the naphthalimide rings on A7. In contrast, the NOEs with the A7·T10 pair are much weaker in dAAAAAA^{AG}, as observed in dTTTTTT^{TG}. The flanking A1·T16−A6·T11 segment of dAAAAAA^{AG} also retains an

(26) Nelson, H. C. M.; Finch, J. T.; Luisi, B. F.; Klug, A. *Nature* **1987**, *330*, 221–6.
(27) Nadeau, J. G.; Crothers, D. M. *Proc. Natl. Acad. Sci. U.S.A.* **1989**, *86*, 2622–6.
(28) MacDonald, D.; Herbert, K.; Zhang, X.; Pologruto, T.; Lu, P. *J. Mol. Biol.* **2001**, *306*, 1081–98.
(29) Barbic, A.; Zimmer, D. P.; Crothers, D. M. *Proc. Natl. Acad. Sci. U.S.A.* **2003**, *100*, 2369–73.
(30) Stefl, R.; Wu, H.; Ravindranathan, S.; Sklenar, V.; Feigon, J. *Proc. Natl. Acad. Sci. U.S.A.* **2004**, *101*, 1177–82.
(31) Woods, K. K.; Maehigashi, T.; Howerton, S. B.; Sines, C. C.; Tannenbaum, S.; Williams, L. D. *J. Am. Chem. Soc.* **2004**, *126*, 15330–1.

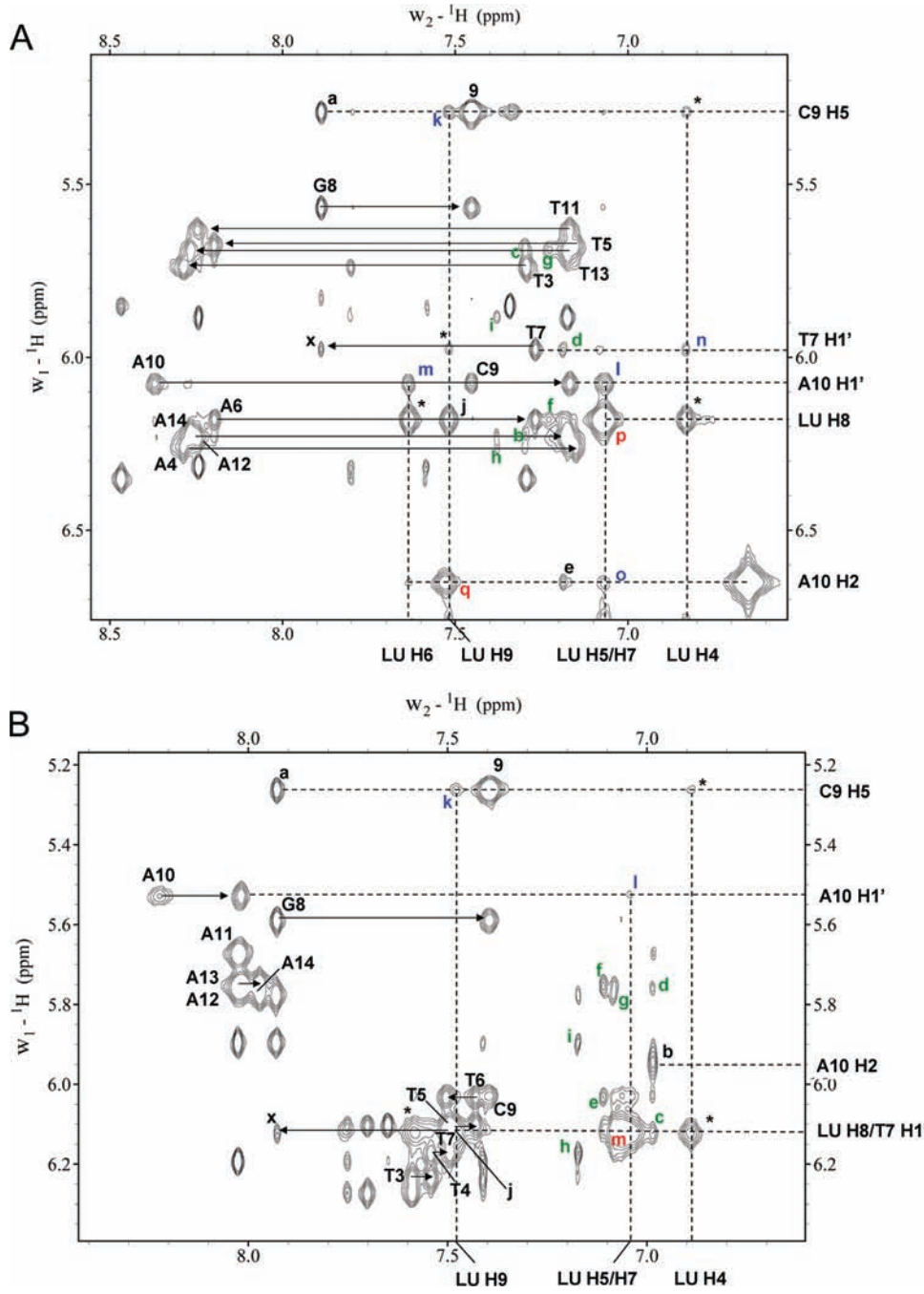

Figure 3. NMR spectra of the dTATATA^{TG}− and dTTTTTT^{TG}−elinafide complexes. Assignment of the aromatic and H1′ NOESY regions (250 ms; mixing time, 25 °C) of dTATATA^{TG} (A) and dTTTTTT^{TG} (B) in the presence of 1.1 and 2.5 equiv of elinafide, respectively. DNA intraresidue H1′−H6/H8 cross-peaks are labeled with residue name and number, intraresidue H5−H6 cross-peaks are labeled with residue number, and sequential NOE connectivities are indicated with horizontal arrows. These connectivities are weaker (marked with ×) or nondetectable for the T7•A10−G8•C9 steps due to LU bisintercalation. In panel A, intramolecular cross-peaks a−j are assigned as follows: a, G8 H8−C9 H5; b, A4 H2−A14 H1′; c, A4 H2−T5 H1′; d, A6 H2−T7 H1′; e, A6 H2−A10 H2; f, A12 H2−A6 H1′; g, A12 H2−T13 H1′; h, A14 H2−A4 H1′; i, A14 H2−T15 H1′; j, LU H8−H9. The blue-labeled k−o cross-peaks are intermolecular: k, LU H9−C9 H5; l, LU H7−A10 H1′; m, LU H6−A10 H1′; n, LU H4−T7 H1′; o, LU H5−A10 H2. The red-labeled p and q cross-peaks are exchange signals, confirmed by ROESY experiments: p, LU H5−H8 (due to ring rotation; overlapped with the LU H7−H8 NOE); q A10 (bound) H2−A10 (free) H2. In B, intramolecular cross-peaks a−j are assigned as follows: a, G8 H8−C9 H5; b, A10 H2−A11 H2; c, A11 H2−T7 H1′; d, A11 H2−A12 H1′; e, A12 H2−T6 H1′; f, A12 H2−A13 H1′; g, A13 H2−A14 H1′; h, A14 H2−T4 H1′; i, A14 H2−A15 H1′; j, LU H8−H9. The blue-labeled k and l cross-peaks are intermolecular: k, LU H9−C9 H5; l, LU H7−A10 H1′. The red-labeled m cross-peak is an exchange signal due to ring rotation, confirmed by ROESY experiments: LU H5−H8 (overlapped with the LU H7−H8 NOE). In panels A and B, LU−LU and DNA−LU NOE cross-peaks mostly mediated by naphthalimide exchange[19] are labeled with asterisks, the NOEs between adenine H2s and H1′ protons are green-labeled, the interactions of important DNA and LU protons are highlighted with dashed lines, and the assignments of the two terminal 1•16 and 2•15 base pairs have been omitted for clarity.

A-tract conformation, but the substantially weaker A6 H2−A7 H1′ (Figure S3, cross-peak g, Supporting Information) and A7 H2−T11 H1′ interactions indicate a disruption of the A-tract structure at the A6•T11−A7•T10 step. Severe broadening is observed for the A7 H2 and H8 aromatic resonances in both dTTATAT^{AG} and dAAAAAA^{AG}. This broadening also affects the aromatic resonances of the neighboring A5, A6, T10, and T11 residues in dAAAAAA^{AG}, suggesting enhanced dynamics of the flanking pairs in this complex (Figure S3, Supporting Information).

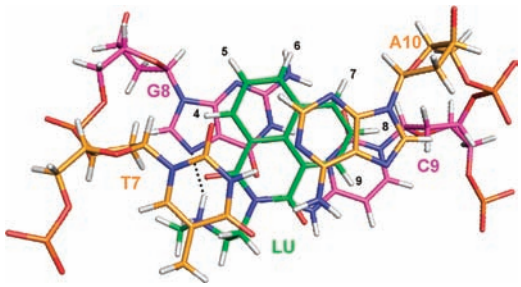

Figure 4. View of an elinafide TGCA binding site. Projection down the helix axis of a TGCA−elinafide complex (PDB 1CX3[19]), showing the naphthalimide ring (with green carbon atoms) intercalated between the T7·A10 base pair (orange carbons) and the G8·C9 base pair (pink carbons). As indicated by NOE contacts[19] (Figure 3), the small naphthalimide rings mostly stack between G8 and A10, showing little overlap with the adjacent pyrimidines. This *interstrand* A10−naphthalimide−G8 stack is substituted with an *intrastrand* A7−naphthalimide−G8 stack in AGCT complexes, as indicated by the dTTATAT^{AG} and dAAAAAA^{AG} NMR analyses (Figure S3, Supporting Information). In both TGCA and ACGT complexes, one of the electronegative imide carbonyls of the drug is brought into unfavorable proximity of the electronegative N7 and O6 atoms of G8 by the strong interactions established by the amino groups of the linker (represented with a black dash line).

Dynamic Effects: Naphthalimide Ring Motion. NMR exchange cross-peaks are observed in all complexes between symmetric and intercalated naphthalimide proton resonances (Figure 3 and Figure S3, Supporting Information), which selectively broaden with increasing temperatures.[19,20] These data are indicative of an unusual process involving 180° rotating motions of the naphthalimide rings,[19,20] which exchange between two equivalent intercalated states at rates ranging from 13 to 32 s^{-1} at 25 °C in the different TGCA and ACGT complexes (Table 1, Figure 5A, and Figure S4, Supporting Information). These ring motions are significantly faster than the 1−4 s^{-1} intercalation dissociation rates measured by NMR spectroscopy at 25 °C (k_d^{int}, Table 1), [20] and much faster than the DNA−ligand dissociation rates obtained by SPR at 25 °C (Table 2A).

The sequences flanking the TGCA and AGCT sites have a significant effect on the rates of intercalated naphthalimide ring rotation. The rotation rates are 2-fold faster in the lower affinity TGCA dTTTTTT^{TG} and dTTATTT^{TG} complexes flanked by A-tracts relative to the dTATATA^{TG} and dTTATAT^{TG} complexes flanked by mostly alternating AT pairs. A similar trend is observed for the AGCT complexes, with dAAAAAA^{AG} having a faster rotation rate than dTTATAT^{AG}, but in this case the differences are smaller (Table 1, Figure 5A, and Figure S4, Supporting Information).

Base-Pair Opening Rates. In order to find out whether the observed trends in binding affinity and naphthalimide ring dynamics are correlated with local and/or cooperative DNA motions, we measured base-pair opening rates in the dTATATA^{TG}, dTTTTTT^{TG}, and dTTATAT^{AG} complexes using imino proton exchange experiments, which are a well-established method for analyzing nucleic acid base dynamics on the millisecond time scale.[22] Several observations can be made on the basis of the data shown in Table 3 and Figure 5B,C. First, the opening rates of the TGCA and AGCT central G8·C9 pairs are significantly slower relative to similar base pairs in free DNA duplexes,[32] as previously observed in other bisintercalation complexes.[33] In addition, these G8·C9 opening rates are in the same range as the naphthalimide ring rotation rates measured in these complexes (compare the k_{rot} and k_{op} values of dTATATA^{TG}, dTTTTTT^{TG}, and dTTATAT^{AG} in Tables 1 and 3, respectively). Second, the T4·A13−T6·A11 segment of dTTTTTT^{TG} exhibits slow opening rates typical of A-tracts[34] (Table 3 and Figure 5C). Third, the opening rates of the 7·10 A·T pairs of the dTTTTTT^{TG} TGCA and dTTATAT^{AG} AGCT binding sites (adjacent to the drug rings) are very fast. In particular, the T7·A10 imino resonance of dTTTTTT^{TG} already broadens out at pH 8.8 without adding any base. In contrast, this pair is more stable in the dTATATA^{TG} complex (Figure 5B). Together with the observation of unusual, nonsequential NOEs involving the dTTTTTT^{TG} T7 and dTTATAT^{AG} and dAAAAAA^{AG} T10 methyl groups (not shown), these data indicate that T7 and T10 expend a considerable amount of time in an opened (extrahelical) conformation in these complexes.

Effect of Ionic Strength. The NMR structure of an ATGCAT−elinafide complex revealed strong hydrogen bonding and electrostatic interactions between the protonated amino groups of the linker and the electronegative groups of guanine in the major groove[19] (Figure 4). These contacts are important for the sequence-specific binding of elinafide to DNA, which preferentially binds guanine-containing sequences as shown above and in previous work.[20] We have further explored the role of the linker interactions by measuring UV thermal stabilizations and ring dynamics in TGCA dTATATA^{TG} and dTTTTTT^{TG} complexes in the presence of 1 M NaCl. The screening effect of the ions reduces the repulsion between DNA phosphate groups, so higher thermal stabilities are observed for both free and bound DNA duplexes (Table 4). However, this effect also reduces the attractive interactions between the aminoalkyl groups of elinafide and the DNA duplexes, so that a substantially lower elinafide-induced thermal stabilization is observed for dTATATA^{TG} (Table 4). This result confirms the importance of the electrostatic interactions established by the elinafide linker. Regarding ligand dynamics, the small effect of the ionic strength on the ring rotation rates indicates that low ΔT_m values are not always accompanied by increased ring dynamics.

Discussion

Elinafide has been shown to be a DNA bisintercalating agent[18,19] with topoisomerase II inhibitory activity and potent cytotoxic properties.[17] However, the structure of its complexes with DNA is not optimal. The drug rings are smaller than those of typical intercalators, and the stacking interactions with the adjacent base pairs of a typical TGCA binding site leave out the pyrimidines, specially the outer T's[19] (Figure 4). Furthermore, the electronic structure of the elinafide rings does not seem to be well-suited for stacking on the G·C pair, because one of the electronegative naphthalimide carbonyls is forced to sit on top of the electronegative O6 and N7 atoms of G by the strong interactions established by the protonated amino groups of the drug linker with this base (Figure 4). These features probably make the DNA interactions of this drug particularly sensitive to indirect readout effects arising from the structural preferences or conformational fluctuations of the bound DNA sequences, as we have shown above.

(32) Kochoyan, M.; Lancelot, G.; Leroy, J. L. *Nucleic Acids Res.* **1988**, *16*, 7685–702.
(33) Leroy, J. L.; Gao, X. L.; Misra, V.; Gueron, M.; Patel, D. J. *Biochemistry* **1992**, *31*, 1407–15.
(34) Snoussi, K.; Leroy, J. L. *Biochemistry* **2002**, *41*, 12467–74.

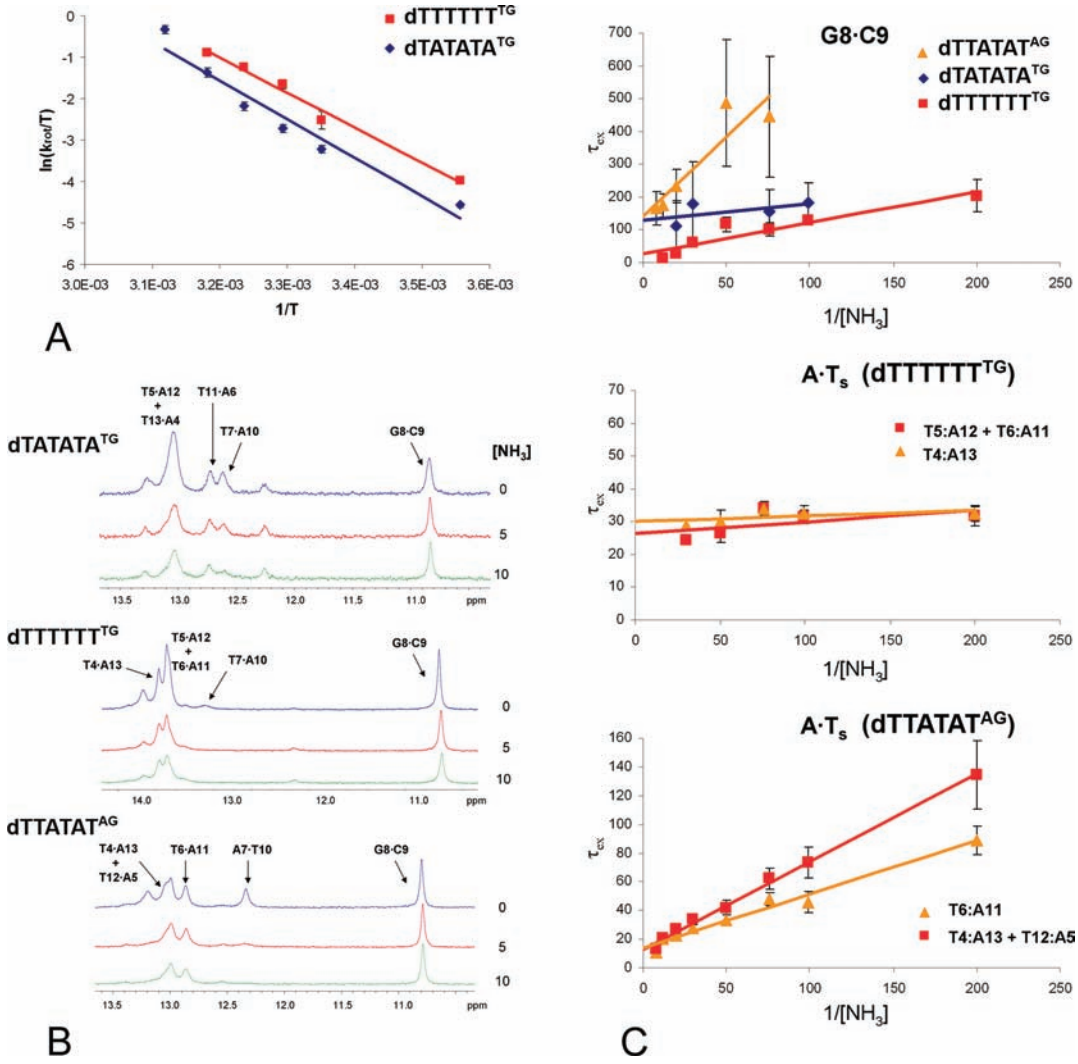

Figure 5. Naphthalimide ring rotation rates and base-pair opening rates. (A) Eyring plots comparing the naphthalimide ring rotation rates (k_{rot}, s^{-1}) as a function of temperature (T, K) in dTTTTTT^{TG} and dTATATA^{TG}. (B) Imino proton region of the ^1H_2O ^1H NMR spectra (600 MHz) of the dTATATA^{TG}−, dTTTTTT^{TG}−, and dTTATAT^{AG}−elinafide complexes at pH 8.8 and 8 °C with no NH_3 added (top) and in the presence of 5 mM (middle) and 10 mM (bottom) NH_3. The assignments of the G8·C9 and flanking T·A iminos are labeled over the resonances. (C) Variation of the imino proton exchange times (τ_{ex}, ms) as a function of the inverse of the ammonia base concentration (1/[NH_3], M^{-1}); the y-intercepts of the linear fits are the base-pair lifetimes ($\tau_{op} = 1/k_{op}$). Top, comparison of the dTTATAT^{AG}, dTATATA^{TG}, and dTTTTTT^{TG} G8·C9 base pairs; middle, dTTTTTT^{TG} flanking T·A base pairs; bottom, dTTATAT^{AG} flanking T·A base pairs.

Table 3. Base-Pair Opening Rates in DNA−Elinafide Complexes[a]

complex[b]	4·13	5·12	6·11	7·10	G8·C9
			TGCA Complexes		
dTATATA^{TG}	[c]	[c]	[c]	∼333 (∼3)[c]	8 ± 2 (129 ± 32)
dTTTTTT^{TG}	33 ± 2 (30 ± 2)	[d]	[d]	≫1000 (≪1)	37 ± 19 (27 ± 14)
			AGCT Complex		
dTTATAT^{AG}	[e]	[e]	77 ± 6 (13 ± 1)	∼1000 (∼1)	7 ± 3 (141 ± 52)

[a] Opening rates (k_{op}, s^{-1}) and lifetimes (τ_{op}, ms; in parentheses) of the 4·13−8·9 base pairs in the dTATATA^{TG}, dTTTTTT^{TG}, and dTTATAT^{AG} complexes at 8 °C and pH 8.8. [b] The sequences of the complexes are shown in Figure 1C, and the DNA:elinafide equivalent ratios are (as required by NMR titrations) as follows: dTATATA^{TG}, 1:1.1; dTTTTTT^{TG}, 1:2.5; dTTATAT^{AG}, 1:1.5. [c] The flanking A·T opening rates could not be accurately determined in this complex. [d] Overlapped T5·A12 + T6·A11 iminos (Figure 5B) with $k_{op} = 38 \pm 4$ s^{-1} and $\tau_{op} = 26 \pm 3$ ms. [e] Overlapped T4·A13 + A5·T12 iminos (Figure 5B) with $k_{op} = 71 \pm 10$ s^{-1} and $\tau_{op} = 14 \pm 2$ ms.

Our results underline the fact that the interaction of this simple molecule with DNA is in fact substantially complex. Overall, the data are consistent with two superposed interactions, one process involving ligand binding to the DNA systems with nanomolar K_d's and 10^{-2} s^{-1} dissociation rates (Figure 2B and Table 2A) and another process of ring intercalation characterized by faster (1−4 s^{-1}) dissociation rates (Table 1)[20] and substantially higher K_d's in some cases (Figure S1, Supporting Information). The DNA sequences influence both events through indirect readout effects, but these effects appear to be particularly relevant for the second (intercalation) process. Because the clearest example is provided by TGCA sites flanked by

Table 4. Impact of Ionic Strength on DNA−Elinafide Interactions: Free (T_m^f) and Bound (T_m^b) DNA Melting Temperatures, Elinafide-Induced Thermal Stabilizations (ΔT_m), DNA−Naphthalimide Intercalation Dissociation Rates (k_d^{int}), and Naphthalimide Ring Rotation Rates (k_{rot}) at 25 °C for the dTATATA^{TG} and dTTTTTT^{TG} Complexes at 1 M NaCl Concentration

TGCA complex[a]	T_m^f (°C)	T_m^b (°C)	ΔT_m (°C)	k_d^{int}[b] (s^{-1})	k_{rot}[b] (s^{-1})
dTATATA^{TG}	53	54	1	8.2 ± 1.7	11 ± 3
dTTTTTT^{TG}	60	60	0	13.6 ± 2.0	30 ± 5

[a] The sequences of the complexes are shown in Figure 1C, and the DNA:elinafide equivalent ratios are (as required by NMR titrations) as follows: dTATATA^{TG}, 1:1.1; dTTTTTT^{TG}, 1:2.5. The thermal denaturation experiments were repeated at least two times for each system, and the average standard deviation for T_m and ΔT_m values is 1 °C. [b] Calculated from NOESY experiments at 25 °C.

alternating AT pairs (dTATATA^{TG}, hATATA^{TG} and hTA^{TG}) or continuous A-tracts on 3′ (dTTTTTT^{TG} and hTTTTT^{TG}), the discussion will focus on these complexes first.

The SPR experiments detect a 10-fold difference between the K_d's of elinafide binding to the higher affinity hTA^{TG} and hATATA^{TG} hairpins and the K_d of the lower affinity hTTTTT^{TG} hairpin flanked by an A-tract: $(2-4) \times 10^{-9}$ versus 2×10^{-8} M (Table 2A). A 5-fold difference in ΔH disfavoring hTTTTT^{TG} is the factor mainly responsible for this K_d difference (Table 2B). If we now analyze the results obtained for equivalent dTATATA^{TG} and dTTTTTT^{TG} duplexes using NMR and UV thermal denaturation experiments, the differences are substantially larger. The intercalation dissociation constant estimated by NMR spectroscopy for dTTTTTT^{TG} using the slowly exchanging free and bound aromatic DNA resonances is $\sim 3 \times 10^{-4}$ M, higher relative to dTATATA^{TG} (Figure S1, Supporting Information), and approximately 10 000-fold higher than the K_d measured by SPR for hTTTTT^{TG} (Table 2A). A large difference between dTATATA^{TG} and dTTTTTT^{TG} is also reflected in the UV thermal stabilizations induced by elinafide binding to these duplexes. The ΔT_m value is 6 °C for dTATATA^{TG}, the highest within the TGCA series, but becomes negligible for dTTTTTT^{TG}. This would translate into at least a 10 000-fold difference between the dTATATA^{TG}− and dTTTTTT^{TG}−elinafide binding affinities calculated from the ΔT_m values (Table S1, Supporting Information).

The apparent discrepancies in the K_d values determined by SPR experiments and UV thermal and NMR experiments are explained by the fact that the two sets of techniques detect two different phases of the interaction: high affinity binding to the double-helical stems and lower affinity (in some sequences) naphthalimide bisintercalation. SPR primarily detects the first process, because this technique is insensitive to the interaction mode and measures changes in the refractive index of the surface as a consequence of the initial elinafide binding to the groove. NMR spectroscopy (and probably UV thermal experiments as well) predominantly detect ring intercalation: the DNA chemical shifts mainly change upon naphthalimide stacking (see Figure 3 and Figures S1 and S3, Supporting Information), and ring intercalation increases the melting temperature of most sequences because the stacking of the naphthalimide system is more stable in a double-helical environment relative to a single-stranded one, as is often the case for intercalative drugs.[25] These conclusions are supported by the fact that, relative to elinafide, the bisfuronaphthalimide MCI3335, containing tetracyclic rather than tricyclic rings, gives rise to very stable NMR intercalation complexes with considerably higher UV ΔT_m values (14 °C; González-Bulnes and Gallego, unpublished results) yet similar 5×10^{-9} M K_d's determined by SPR.[14]

A comparison of the rest of the complexes confirms that the sequences flanking the TGCA and AGCT binding sites have a large impact on ΔT_m values (Table 1 and Table S1, Supporting Information). The most important factor governing the ΔT_m's appears to be the formation of an A-tract of at least four nucleotides on the 3′ side of TGCA (as in dTTTTTT^{TG} and dTTATTT^{TG}). If this condition is fulfilled, then ΔT_m becomes very low. Even changes in one flanking nucleotide can cause drops of 3 °C in ΔT_m if they are conducive to the formation of this four-nucleotide tract (compare dTTATAT^{TG} and dTTATTT^{TG} in Table 1). The effect of the flanking A-tracts also depends on their orientation with respect to the binding site. When the A-tract is on the 3′ side of the GC site (as in dTTTTTT^{TG} and dTTATTT^{TG}) the deleterious effects on affinity are much stronger than for complexes with A-tracts neighboring the 5′ side of the GC site (as in dAAAAAA^{AG}) (Table 1).

A particularly interesting question concerns the molecular mechanism of A-tract indirect discrimination, because this is relevant to the sequence-specific binding of other small molecules and proteins to DNA. The stacking contacts between the naphthalimide rings and the adjacent T7·A10 and A7·T10 pairs are weaker in the dTTTTTT^{TG} and dAAAAAA^{AG} complexes flanked by A-tracts, respectively, relative to complexes flanked by alternating AT pairs such as dTATATA^{TG} and dTTATAT^{AG}. In addition, the A-tract conformation of the flanking pairs is interrupted at the dTTTTTT^{TG} T6·A11−T7·A10 and dAAAAAA^{AG} A6·T11−A7·T10 steps (Figure 3 and Figure S3, Supporting Information). The base-pair opening rate of the T7·A10 pair is anomalously fast in dTTTTTT^{TG}, significantly faster relative to the same pair in dTATATA^{TG} (Table 3 and Figure 5B). Increased broadening is also observed for the nonexchangeable resonances of the 7·10 pair in dTTTTTT^{TG} and dAAAAAA^{AG} relative to dTATATA^{TG} and dTTATAT^{AG} (Figure 3 and Figure S3, Supporting Information). Together with the unusual, nonsequential NOEs detected for the T7 methyl group of dTTTTTT^{TG}, these data suggest that T7 frequently adopts an opened (extrahelical) location in this complex.

The weaker intra- and intermolecular stacking contacts observed in dTTTTTT^{TG} and dAAAAAA^{AG} are consistent with the lower ΔH value measured by SPR for the hTTTTT^{TG} hairpin relative to hATATA^{TG} and hTA^{TG} and are probably the basis for flanking A-tract discrimination by elinafide, highlighting the importance of stacking interactions for DNA stability. There are NMR and X-ray structures of A-tracts located on both the 3′ side of unbound GC steps (as in dTTTTTT^{TG}) and the 5′ side (as in dAAAAAA^{AG}).[26,28−31] A-tracts contain separate stacks of negatively inclined and maximally overlapped adenine and thymine bases that are accommodated at the T_nG and A_nG junctions through base-pair buckling. In addition, the helix axis bends toward the major groove via positive roll angles at these junctions, which are precisely the steps where the naphthalimides rings of elinafide need to intercalate. In dTTTTTT^{TG}, the naphthalimide rings try to stack between G8 and the A10 base of the *opposite* strand (Figure 4), but this leads to loss of stacking contacts between T7·A10 and the adjacent A-tract (Figure 3) and to very fast T7·A10 opening rates (Figure 5B). Better A_n−A7 and A7−naphthalimide−guanine *intrastrand* stacking

interactions probably explain the smaller deleterious effect of the A-tract located on the 5′ side of the dAAAAAA^{AG} GC binding site (Figure 3 and Figure S3, Supporting Information). In either case, the elinafide rings need to disrupt a stable structure with slow base-pair opening rates in order to bisintercalate at the A-tract−GC junctions. Since the intercalation dissociation rates are not particularly sensitive to the flanking sequences (Table 1),[20] the ring association rate appears as a likely important factor modulating the efficiency of naphthalimide intercalation, at least in TGCA sites (Table 2A).

Superposed with the DNA duplex-binding and ring intercalation processes described above is a third, unusual dynamic process that adds further complexity to the DNA−elinafide interaction. The naphthalimide rings exchange via 180° rotating motions between two equivalent intercalated states in all complexes. This process occurs at rates (13−32 s^{-1}) significantly faster than intercalation dissociation rates (Table 1)[20] and much faster than DNA−ligand dissociation rates (Table 2A) and is also modulated by the sequence of the flanking base pairs (Table 1). Sequences containing flanking A-tracts give rise to less stable complexes, enhanced DNA dynamics, and faster naphthalimide ring rotation rates. The correlation between ΔT_m and ring rotation rates is not always applicable (e.g., dTATATA^{TG} can exhibit low k_{rot}'s and ΔT_m's, Table 4), indicating that intrinsic factors related to DNA dynamics or stability are involved in the mechanism of naphthalimide ring flipping, as proposed previously.[20] In fact, the rates of intercalated ring rotation are in the same range as the opening rates of the central G8·C9 pairs of dTATATA^{TG}, dTTTTTT^{TG}, and dTTATAT^{AG} (Tables 1 and 3), suggesting that both processes may be coupled.

The findings described in this paper may have pharmacological implications. The small and electronically flawed structure of the naphthalimide rings of elinafide translates into very fast opening rates of the outer A·T pairs of TGCA and AGCT binding sites together with ring flipping dynamics. In addition, the intercalation of the drug rings is unstable in sites flanked by A-tracts. The conformational fluctuations of the DNA (probably associated with pyrimidine unstacking) or the transient presence of one or two hydrophobic rings of the drug in the major groove may be an advantage for antitumor drug design if they are recognized by effector proteins or enzymes acting on DNA. Further work will be needed to test this hypothesis.

Acknowledgment. This work was supported by Ministerio de Educación y Ciencia of Spain (Ramón y Cajal contract and Grant SAF2007-60243 to J.G.) and the CIPF. We thank Lorena Pérez for excellent technical assistance and Federico Gago for critical reading of the manuscript.

Supporting Information Available: dTATATA^{TG} and dTTTTTT^{TG} NMR spectroscopy titrations, hTA^{TG} and hATATA^{TG} SPR experiments, dTTATAT^{AG} and dAAAAAA^{AG} NOESY spectra, dTTATAT^{TG}, dTTATTT^{TG}, dTTATAT^{AG}, and dAAAAAA^{AG} Eyring plots, and UV-determined DNA−elinafide dissociation constants.This material is available free of charge via the Internet at http://pubs.acs.org.

JA901505P